Available online at www.sciencedirect.com
ScienceDirect
International Journal of Heat and Mass Transfer 50 (2007) 2521–2536
International Journal of HEAT and MASS TRANSFER
www.elsevier.com/locate/ijhmt

Cross flow heat exchange of textile cellular metal core sandwich panels

J. Tian [a], T.J. Lu [b,*], H.P. Hodson [a], D.T. Queheillalt [c], H.N.G. Wadley [c]

[a] Department of Engineering, University of Cambridge, Cambridge CB2 1PZ, UK
[b] MOE Key Laboratory of Strength and Vibration, School of Aerospace, Xian Jiaotong University, Xian 710049, PR China
[c] Materials Science Department, University of Virginia Charlottesville, VA 22904, USA

Received 11 January 2006; received in revised form 23 November 2006
Available online 6 March 2007

Abstract

This paper presents a combined experimental and theoretical study on the thermal–hydraulic performance of a novel type of periodic textile cellular structure, subjected to forced convection using both air and water as a coolant. The samples were fabricated as sandwich panels, with the textile cores bonded to two solid face-sheets using a brazing alloy. These efficient load supporting sandwich structures can also be used for active cooling. The effects of cell topology, pore fraction and material properties (high thermal conductivity copper or low thermal conductivity stainless steel) on both coolants flow resistance and heat transfer rate were measured. The flow friction factor is found to depend mainly on the open area ratio in the flow direction (which is dependent upon cell topology and pore fraction), whilst the amount of heat transferred is dependent upon solid conductivity, pore fraction and surface area density. Analytical models were used to develop predictive relations between both the pressure loss and heat transfer performance for different textile geometries. Good agreement between the predictions and measurements were obtained. Due to high thermal capacity of water, it was found that the model for water cooling must account for the additional contribution due to thermal dispersion. The dispersion conductivity was found to be related to coolant property, local flow velocity, wire diameter and pore fraction. Finally, the thermal performance of brazed woven textiles is compared with other heat exchanger media, such as open-celled metallic foams and louvered fins.

Keywords: Woven textile; Forced convection; Pressure loss; Heat transfer; Fin analogy; Thermal dispersion; Thermal efficiency

1. Introduction

Lightweight all-metallic sandwich structures with periodic truss or prismatic cores (Fig. 1) have recently been suggested for simultaneous load bearing and active cooling [1]. The load bearing characteristics of these structures have been well studied, demonstrating the role of cell topology, relative density and parent material properties upon the mechanical performance [1–6]. The continuous channels of these open core structures also allow internal fluid transport, enabling simultaneous active cooling. Several mechanisms contributing to heat transfer have been identified, including low thermal resistance conduction paths from a hot face-sheet through the core, high surface area contact between the core and a coolant, and high heat transfer between the metal surface and the fluid coolant. The focus of this paper is on the thermal performance of sandwiches having brazed woven textile cores under forced convection: structures are fabricated from metal with widely differing thermal conductivities (copper and stainless steel). We investigate the thermal performance of periodic truss cores fabricated by the brazing of metal textiles using both air and water as a coolant.

Woven metallic structures (textiles) have been widely used in aerospace, chemical engineering, food processing, air conditioning/refrigeration, medicine, and so on [7]. Heat dissipation media have three important characteristics: thermal conductivity, pressure loss and heat transfer rate [8]. Analytical and empirical correlations between these characteristics and the overall heat transfer performance have been developed for many structures [9–20].

* Corresponding author. Tel.: +86 29 82665600; fax: +86 29 82668234.
E-mail address: tjlu@mail.xjtu.edu.cn (T.J. Lu).

0017-9310/$ - see front matter © 2007 Elsevier Ltd. All rights reserved.
doi:10.1016/j.ijheatmasstransfer.2006.11.042

Nomenclature

A, A_{cy}	heating area $= LW$, cylinder cross-sectional area
c_p	specific heat of fluid
C_H	tortuous coefficient
D, d_p, D_h	wire diameter, unit cell length, hydraulic diameter
f	friction factor
H, h, d	channel height, local heat transfer coefficient, thermal conductivity
K_{cell}	pressure loss coefficient based on unit cell size
L	channel length
$\dot{m}$	mass flow rate
n, N	number of parallel wires along channel height, mesh number
P, ΔP	pressure and pressure drop over length L
Q, q	input heat, input heat flux
q_0	total heat removal
$q_{parallel}$	heat removed by parallel cylinders
$q_{vertical}$	heat removed by vertical cylinders
q_w	heat transferred between face-sheet and coolant
R_{open}	open area ratio
Re	Reynolds number
T	temperature
U_m	mean velocity
W, w	channel width, aperture width

Greek symbols

ξ	local coordinates along cylinder
ρ	density
α	surface area density
ε	porosity

Subscripts

0	inlet
cy	cylinder
d	dispersion
eff	effective
f	fluid
m	mean
p	parallel
s	solid
sf	surface
v	vertical
w	substrate

For example, Wirtz et al. [9–13] investigated the thermal and fluid flow characteristics of single layer woven textiles, rows of serpentine-pattern screens, and regularly stacked (but not bonded) three-dimensional (3D) metal textile sheets. It was found that the performance of these textile structures was comparable to plate-fins. The wire cross-over's in these structures were not bonded and while they may be used as heat exchangers, node rotation precludes their use as structural members. In addition, the unbonded nodes result in a high thermal resistance at the nodes, which reduces their thermal spreading performance. Jiang et al. [21,44] conducted both experimental and numerical studies of forced convective heat transfer in packed beds of sintered and non-sintered copper spheres, and found that sintering significantly increases the overall heat transfer rate due to reduced thermal contact resistance. The

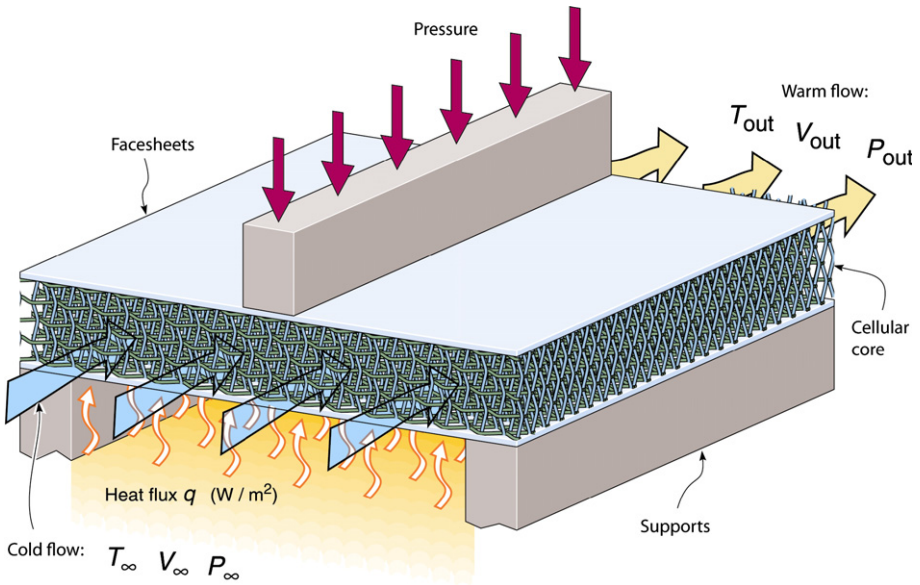

Fig. 1. Sandwich construction with textile technology: (a) a transient liquid phase joins the wire mesh screen laminated at all points of contact; (b) face-sheets are added to the textile core.

increases could be large: up to 15 times for water and 30 times for air [21]. We note that such bonding also dramatically modifies the mechanical properties and creates opportunities for multifunctional applications of the type recently envisioned [6].

Sandwich panels with textile cores have recently been fabricated using a transient liquid phase (TLP) bonding (brazing) method to create robust nodes at wire cross-overs and between the lamina [7]. It was discovered that the forced air convective thermal efficiency of the brazed textile structures was approximately three times larger than that of open-celled metal foams, principally because much of the lower pressure drop encountered during coolant propagation through collinear pores in the periodic textile structure [7].

In the present study, all-metallic sandwich panels with woven textile cores having diamond or square-shaped pores are tested using both forced air and water as the coolant for a cross-flow heat exchange experiment. A pressure drag model is developed to relate the measured flow resistance across the textile cores topology. A fin analogy model was constructed to characterize the heat transfer performance. Similar fin models have been successfully used to study forced air convection through other porous media [22–26]. However, the water introduces an additional effect (thermal dispersion [27]), which is included in the present model. Finally, the overall heat transfer performances of the textile topology structures are compared with other heat dissipation media including metal foams, truss structures, louvered fins and corrugated ducts.

2. Test sample topology

2.1. Sample fabrication

Individual mesh layers are stacked peak-to-peak such that the textile openings are aligned with each other and joined together at all points of wire contact, either by a brazing alloy in the case of the copper cores or a transient liquid phase (TLP) alloy in the case of the stainless steel cores, creating the cellular metal core. The textile cores are subsequently machined to size by electro-discharge machining and, then, solid face-sheets are added via a second brazing/TLP operation creating the sandwich structure. Fig. 1 illustrates the use of the constructed sandwich laminate with woven textiles for simultaneous structural load bearing and cross-flow heat exchange applications; additional details on sample preparation can be found in [4,5].

Sandwich structures were fabricated with the wire struts either parallel or perpendicular (0/90°), or inclined (±45°) to the face-sheets. When the struts were oriented 0/90° to the face-sheets (Fig. 2a) the samples are designated S; whereas when the struts were oriented ±45° to the face-sheets (Fig. 2b) these samples are designated D. All samples had a width $W = 40$ mm, a core height $H = 10$ mm, a length $L = 60$ mm, and face-sheet thickness of 0.813 mm. Details of the samples tested in this paper are listed in Table 1.

2.2. Unit cell topology

The woven mesh has a wire diameter d, aperture width w, and screen layer thickness $t = 2d$ (Fig. 2). The number of pores per unit length, N (mesh number), is:

$$N = \frac{1}{d + w} \tag{1}$$

For the present samples, N takes the value of 8, 10 and 12 pores/in. With ρ denoting the density of the mesh, the relative density $\bar{\rho}$ of the stacked textile core is:

$$\bar{\rho} \equiv \frac{\rho}{\rho_s} = \frac{\pi N d^2}{2t}\sqrt{1 + \left(\frac{1}{1 + w/d}\right)^2} \tag{2}$$

where ρ_s is the density of the parent solid material and the effect of added weight of the bonding agent at the contact points has been neglected. The pore volume fraction ε of the core is related to $\bar{\rho}$ by:

$$\varepsilon = 1 - \bar{\rho} \tag{3}$$

The surface area density α_{sf} (total surface area per unit volume) is given by:

$$\alpha_{sf} = \frac{\text{total surface area}}{\text{volume}} = \frac{\pi}{w + d} = \pi N \tag{4}$$

3. Experimental test set-up

Two types of coolant were used in this study, air and water (Table 2). Due to the special sealing requirement for water, two different test facilities were used, as described below.

3.1. Test set-up and data acquisition procedures for forced air convection

A schematic illustration of the forced air convection test facility is shown in Fig. 3a. Air is drawn through a rectangular channel, in which the textile based sandwich structure was fitted. The coolant flows through a layer of wire screen meshes, followed by a 4:1 contraction, a flow straightening honeycomb layer, another wire screen layer and a relatively long parallel plate channel before it reaches the sample. An iso-flux boundary condition was imposed on the bottom face-sheet of the sandwich structures via a heating pad, while the top face-sheet was thermally insulated. A pure copper heat spreader plate, 0.9 mm thick, was inserted between the heating element and the bottom face-sheet.

3.2. Test set-up and data acquisition procedures for forced water convection

For forced water convection experiment, the testing facility (schematic shown in Fig. 3b) of Prof. P.X. Jiang

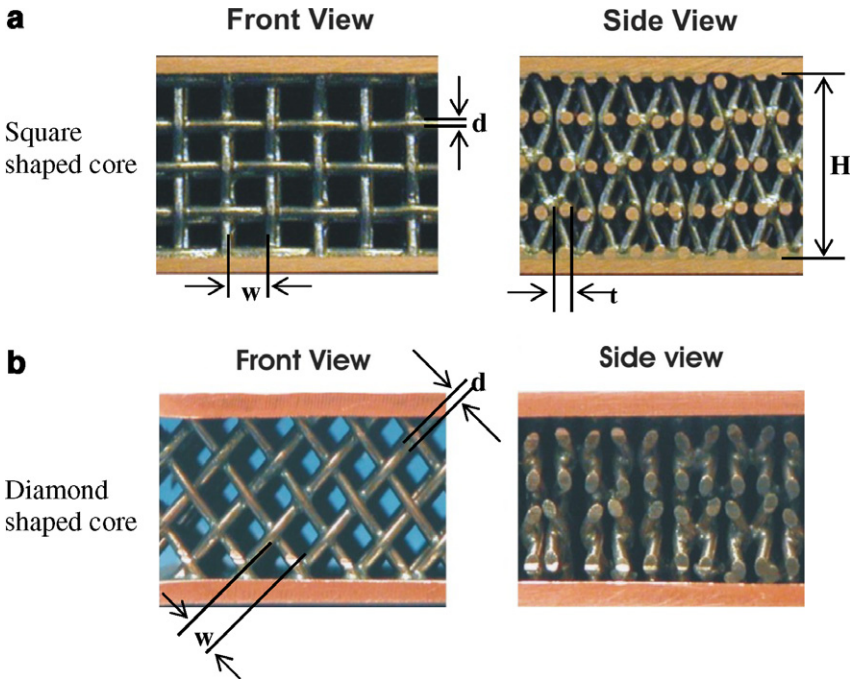

Fig. 2. Two prototype textile laminate heat exchangers: (a) images of square-shaped pores; (b) images of diamond-shaped pores.

Table 1
Morphological parameters for test samples

Test sample	Material	Wire diameter (mm)	Aperture (mm)	Porosity	Surface area density (m^2/m^3)	Open area ratio
S-1 & D-1	Copper	0.8	2.36	0.795	994	0.5577
S-2 & D-2		1.0	2.13	0.737	1004	0.4631
S-3 & D-3		1.2	1.98	0.683	988	0.3876
S-4 & D-4		0.8	1.30	0.680	1496	0.3832
S-6 & D-5	Stainless steel	0.9	2.275	0.769	989	0.5134
S-7 & D-6		0.56	1.98	0.822	1237	0.6076
S-8 & D-7		0.56	1.557	0.785	1470	0.5409

Table 2
Experimental operating conditions

Parameters	Ranges	
Coolant	Air	Water
Inlet coolant velocity	1.0–10 m/s	0.02–0.5 m/s
Reynolds number Re_H	700–10000	100–8000
Inlet temperature	290 K	290 K
Outlet temperature	300–310 K	300–350 K

at Tsinghua University, China, was used. It consists of four major components: water supply, experimental test section, heating arrangement, and data acquisition system. A snake-shaped thin nichrome plate was used as the heating element, which was operated in a way such that constant heat flux is maintained, with negligible temperature change (~0.09 K) across the thickness of the ~1 mm thick copper heat spreader atop the heating element [37]. The amount of heat released from the heating element was adjusted by changing the supply voltage. Consequently, constant heat flux boundary condition was assumed.

Two T-type copper-constantan thermocouples were buried into grooves on the top copper face-sheet to measure the local sample temperature. Additional thermocouples were used to measure the inlet and outlet fluid temperatures. For pressure measurements, a high-resolution manometer was used, while the mass flow rate was obtained by the mass weight method.

3.3. Data reduction parameters

The Reynolds number and friction factor based on the channel height H are defined as:

$$Re_H = \rho_f U_m H/\mu_f \tag{5}$$

$$f = \left(\frac{\Delta P}{L}\cdot H\right)\cdot\left(\frac{1}{\rho_f U_m^2/2}\right) \tag{6}$$

where U_m is the mean coolant velocity at the inlet of a test section of length L, ρ_f and μ_f are the coolant density and viscosity, and $\Delta P/L$ is the pressure drop per unit length. The heat transfer coefficient at any location x along a sandwich panel heated on one face is:

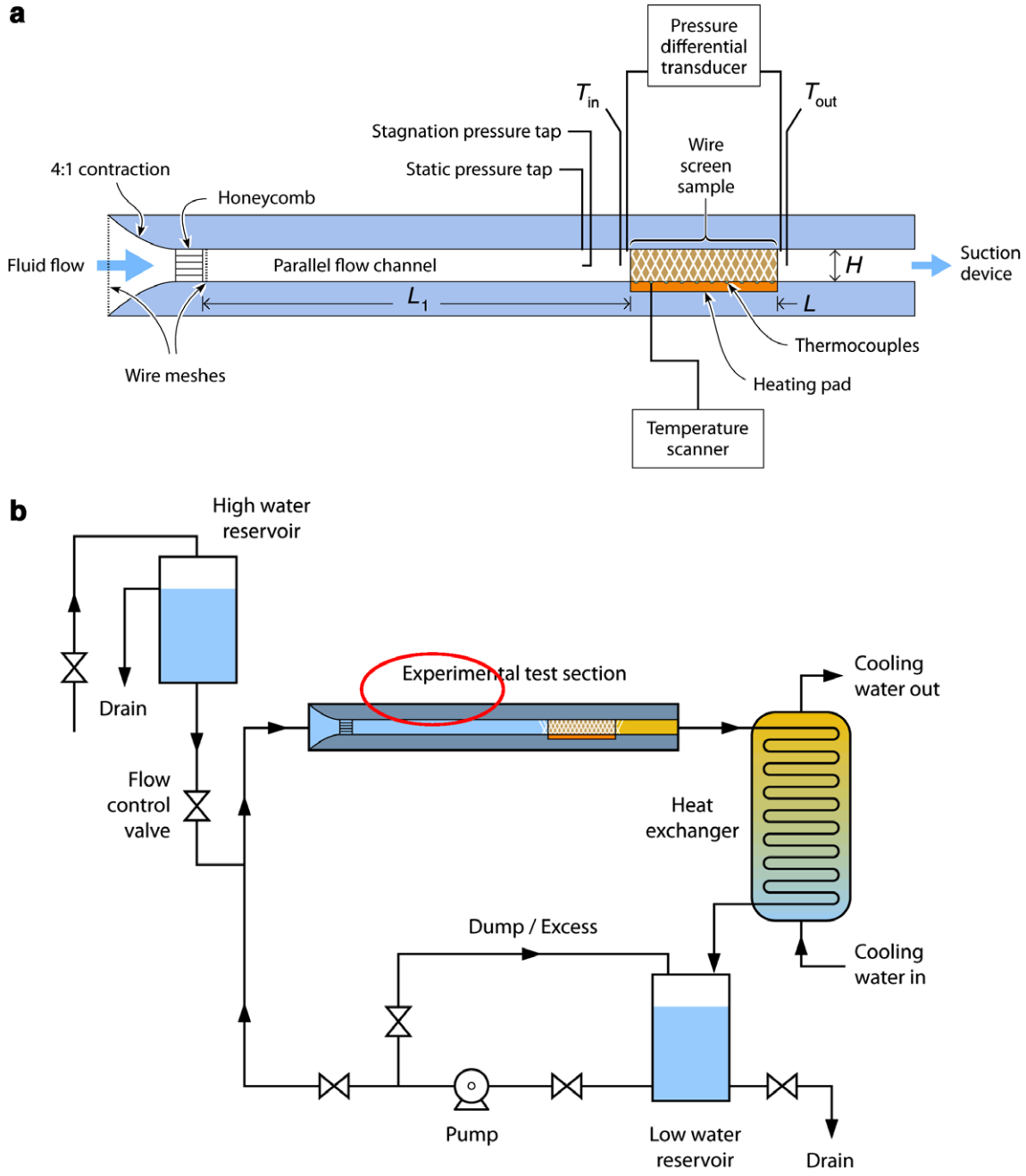

Fig. 3. Experimental set-up for: (a) forced air convection; (b) forced water convection.

$$h_x = \frac{Q/A}{T_w(x) - T_{f,bulk}} \tag{7}$$

where k_f is the thermal conductivity of the coolant, Q is the rate of heat input, A is the heated area, T_w is the temperature of the bottom face-sheet, and $T_{f,bulk}$ is the bulk mean temperature of the coolant at the inlet. Integration along the length of the panel gives the overall heat transfer coefficient $\bar{h}$. The corresponding Nusselt number for the panel is

$$Nu_H = \bar{h}H/k_f \tag{8}$$

3.4. Measurement uncertainty

All measurements were performed under steady-state conditions and repeated until significant data repetition was ensured. An uncertainty analysis was performed by using the method described in [38]. To minimize heat loss, the external surface of the heating element was covered with a thermal insulation material having a very low thermal conductivity ($k = 0.032$ W/mK). In typical operating conditions, the heat loss through the insulation materials was estimated to be less than 2% out of a total imposed heat flux. Further details associated with this estimation

can be found in [37]. The variation in air conductivity, k_f, is negligible in the operating temperature range of 293–303 K, whereas its density, ρ_f, varies by about 5%. The uncertainty in pressure drop measurement was less than 5%. The uncertainties calculated from the root-square method for the mean heat transfer coefficient, Reynolds number and Nusselt number were estimated to be less than 5.3%, 5.7% and 5.4%, respectively.

For the forced water convection, the time that the fluid with a fixed weight passed through was recorded by a stopwatch (0.01 s resolution). The uncertainty of the Reynolds number was estimated to be 4%. The uncertainties of friction factor, heat transfer coefficient and Nusselt number are 4.1%, 8.4%, 8.4%, respectively.

4. Analytical modelling

4.1. Pressure drag model

In the form dominant regime, the friction factor of a cellular core sandwich is a simple function of the core open area ratio [7]:

$$R_{\text{open}} = \text{Open area/Total area} \tag{9}$$

where the open area and the total area are separately the void area in the plane perpendicular to the flow and the frontal area of the sample viewed in the direction of flow (Table 1). The pressure loss coefficient K_{cell} can be computed as [7]

$$K_{\text{cell}} = \frac{\Delta P_{\text{cell}}}{\rho U_m^2/2} = \left(\frac{\Delta P}{L}\cdot d_p\right)\cdot\left(\frac{1}{\rho U_m^2/2}\right) = \left(\frac{1-R_{\text{open}}}{R_{\text{open}}}\right)^2 \tag{10}$$

with $d_p = t = 2d$ is the unit cell length. Combining (6) and (10), the friction factor, f, based on channel height H can be obtained as

$$f = \left(\frac{\Delta P}{L}\cdot H\right)\cdot\left(\frac{1}{\rho U_m^2/2}\right) = \left(\frac{1-R_{\text{open}}}{R_{\text{open}}}\right)^2 \frac{H}{d_p} \tag{11}$$

4.2. Fin analogy model

The problem to be analysed is forced convection through a sandwich panel heat sink whose core has a topology derived from a brazed metal textile lay-up. The channel has length L along the x-axis, core height H in the y-axis and a core width W in the z-axis. At the bottom surface (y=0), a constant heat flux is supplied, while the top surface ($y = H$) is thermally insulated. The coolant flow is parallel to the x-axis, and perpendicular to the textile layers. Thermal physical properties such as thermal conductivity, density and viscosity are assumed to be independent of temperature. Built upon the recent experimental work [31], it is further assumed that fully developed heat and fluid flow is achieved.

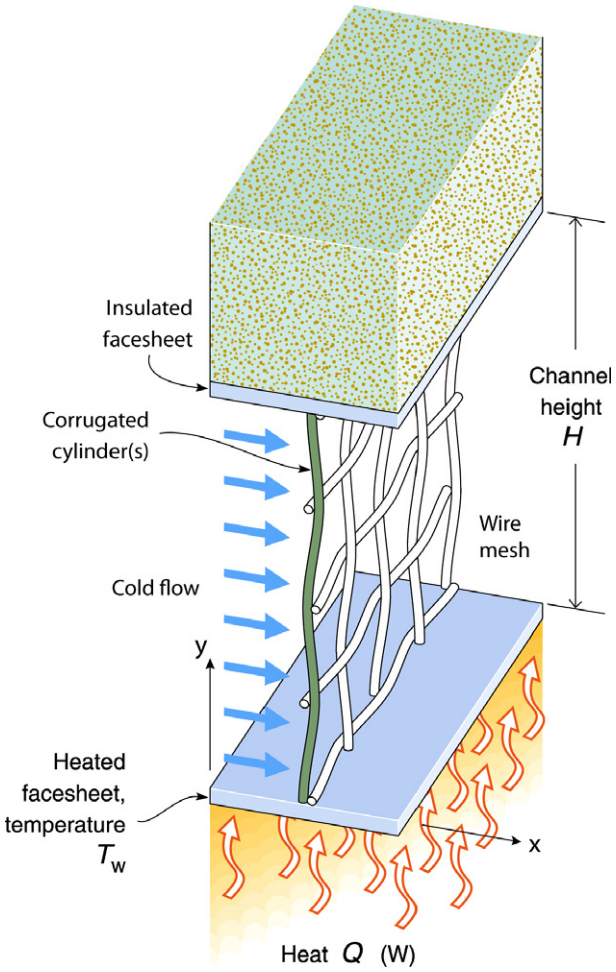

Fig. 4. Single corrugated cylinder.

According to the fin analogy theory, the variation of temperature T along the length of a corrugated cylinder (Fig. 4) is governed by:

$$\frac{d^2T}{d\xi^2} - \frac{4h}{k_s d}(T - T_f) = 0 \tag{12}$$

where h is the interfacial heat transfer coefficient, k_s is the solid conductivity, $T_f(x)$ is the mean fluid temperature at location x, and ξ is a local coordinate along the cylinder with origin $\xi = 0$ at $y = 0$ and $\xi = C_H H$ at $y = H$. Here, C_H is the tortuosity coefficient, with $C_H = \sqrt{1 + d^2/(d+w)^2}$ for square-oriented cores and $C_H = \sqrt{2}\cdot\sqrt{1 + d^2/(d+w)^2}$ for diamond-oriented cores.

A constant heat flux wall boundary condition was assumed, with uniform heat flux $q = Q/A$ supplied at the bottom surface of the cylinder and thermal insulation ($q = 0$) at the top:

$$-k_s\left.\frac{dT}{d\xi}\right|_{\xi=0} = q \quad \text{and} \quad k_s\left.\frac{dT}{d\xi}\right|_{\xi=C_H H} = 0 \tag{13}$$

Subjected to these boundary conditions, (11) can be solved, resulting in:

$$T - T_f = \frac{q}{mk_s}\frac{\cosh(mC_H H - m\xi)}{\sinh(mC_H H)} \tag{14}$$

where $m = \sqrt{4h/(k_s d)}$ is non-dimensional. The wall temperature can be obtained as:

$$T_w - T_f = \frac{q}{mk_s}\frac{\cosh(mC_H H)}{\sinh(mC_H H)} \tag{15}$$

To fully determine T_w, the mean fluid temperature T_f and heat flux q need to be known.

The struts in samples with diamond-oriented cores are mostly connected to the top and bottom face-sheets (edge effects preclude all struts from making contact), whereas half of the struts in samples with square-oriented cores are connected to both the top and bottom face-sheets, with the remaining half parallel to the face-sheets and not directly contacting either face-sheet. Because these transverse wires are bonded to the vertical ones and because the side walls are thermally insulated, it may be assumed that their temperature is the same as that at the contact point with the vertical wire and can be estimated using (14). The fluid temperature surrounding a vertical cylinder at location x can then be obtained by considering energy balance for a control volume of length dx, width W and height H, yielding:

$$\begin{aligned}\dot{m}c_p\Delta T_f(x) &= N_s q_{vertical} A_{cy,v}\mathrm{d}xW + q_w(x)A_w + q_{parallel}A_{cy,p}\mathrm{d}x/t \\ &\equiv q_0\mathrm{d}xW \quad \text{(Square-orientation)} \end{aligned} \tag{16a}$$

$$\begin{aligned}\dot{m}c_p\Delta T_f(x) &= N_s q_{vertical} A_{cy,v}\mathrm{d}xW + q_w(x)A_w \\ &\equiv q_0\mathrm{d}xW \quad \text{(Diamond orientation)} \end{aligned} \tag{16b}$$

where $\dot{m}$ is the mass flow rate, c_p is the specific heat of the fluid, A_{cy} is the cross-sectional area of the cylinder, subscripts v and p stand for vertical and parallel respectively, A_w is the face-sheet area excluding those of the attached cylinders, N_s is the number of vertical cylinders per unit area, $q_{parallel}$ is the heat removed by cylinders parallel to the face-sheets, $q_{vertical}$ is the heat removed by a single vertical cylinder, q_0 is the total heat removal, and q_w is the heat transferred between the face-sheet and the coolant flow, given by:

$$q_w(x) = h_w(T_w(x) - T_f(x)) = h_w\frac{q}{mk_s}\frac{\cosh(mH)}{\sinh(mH)} \tag{17}$$

In (17) h_w is the wall heat transfer coefficient of an empty channel, given by [8,23,24]:

$$h_w = 0.023 Re_{D_h}^{0.8} Pr^{0.4} k_f/D_h \tag{18}$$

where Pr is the Prandtl number and Re_{D_h} is the Reynolds number based on the hydraulic diameter $D_h = 2WH/(W+H)$. Table 3 lists the thermo-physical constants for two coolants (air and water) and two metals (stainless steel and copper) used in this study.

For the interfacial heat transfer coefficient h in (12), it is assumed that the correlation developed by Zukauskas [28] for in-line cylinder arrays in cross-flow may be employed:

Table 3
Thermo-physical constants

Parameters	Air	Water (Depend on temperature)
Density (kg/m^3)	1.1614	997.1–999.1
Dynamic viscosity (kg/ms)	0.00001846	0.000891–0.001137
Specific heat (J/kg K)	1006	4179–4186
Prandtl number	0.71	6.21–8.13
Thermal conductivity (W/mK)	0.025	0.59
	Copper	Stainless steel
Thermal conductivity (W/mK)	380	16.2

$$h = \begin{cases} 0.9Re_d^{0.4}Pr^{0.36}(k_f/d), & 1 \leqslant Re_d < 100 \\ 0.52Re_d^{0.5}Pr^{0.36}(k_f/d), & 100 \leqslant Re_d < 1000 \\ 0.27Re_d^{0.63}Pr^{0.36}(k_f/d), & 1000 \leqslant Re_d < 2\times 10^5 \end{cases} \tag{19}$$

where $Re_d = \rho_f U_m d/\mu_f$ is the Reynolds number based on cylinder diameter d.

For sandwich structures with either square- or diamond-oriented cells, (12) to (19) are sufficient to determine h_x defined in (7), which is then used to calculate $\bar{h}$.

5. Results and discussion

The three non-dimensional parameters of interest are the Nusselt number, Reynolds number and friction factor, all based on channel height H, summarized by:

$$Nu_H = \frac{\bar{h}H}{k_f} \qquad Re_H = \frac{\rho_f U_m H}{\mu_f} \qquad f_H = \frac{(\Delta p/L)H}{\rho_f U_m^2/2} \tag{20}$$

Note that the length scale H is somewhat arbitrary, but selected to facilitate comparisons among sandwich heat sinks with different core topologies. The value of Nu_H depends on the core topology and relative density, as well as the solid and fluid properties. It embodies three different heat transfer mechanisms: conduction through the core struts, core-to-fluid convection, and face-sheet-to-fluid convection. The challenge is to ascertain the heat transfer coefficient and the pressure drop for each of the core topologies over a wide range of Reynolds numbers. The protocol relies on knowledge of the point-wise heat transfer characteristics of the constituent elements of the panel.

5.1. Pressure loss

The experimental results for the friction factor f_H are shown in Figs. 5 and 6 for forced air and water convection, respectively. For forced air convection, nearly all test data fall in the turbulent region, with the friction factor equal to a constant as shown in Fig. 5. For forced water convection, the flow remains laminar until the Reynolds number exceeds ~2000, with a distinct laminar-turbulent transition regime on the f_H versus Re_H plots in Fig. 6.

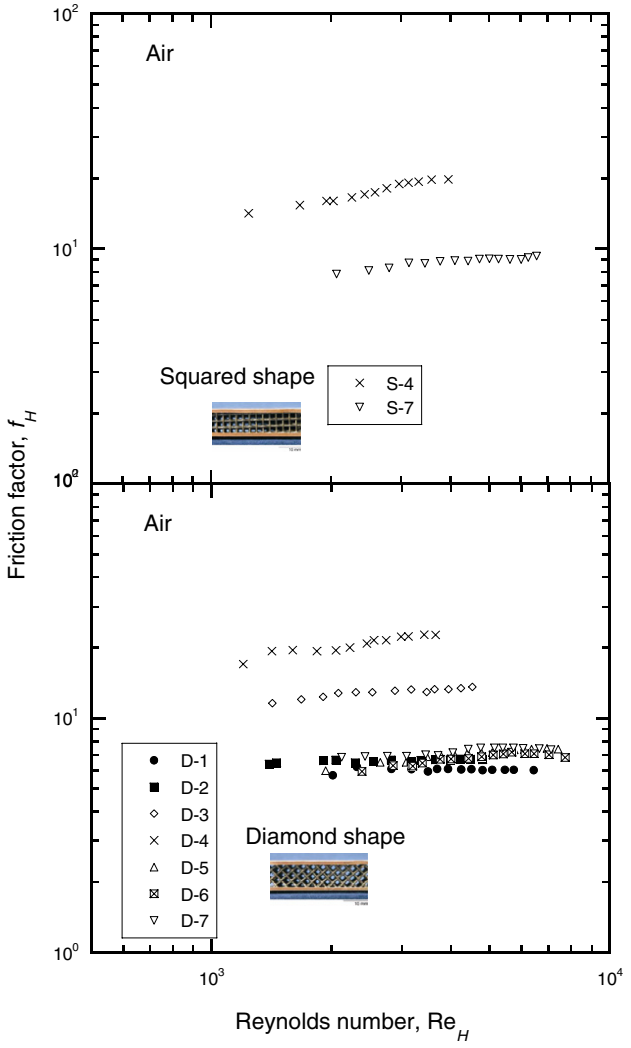

Fig. 5. Friction factors based on channel height (air as coolant).

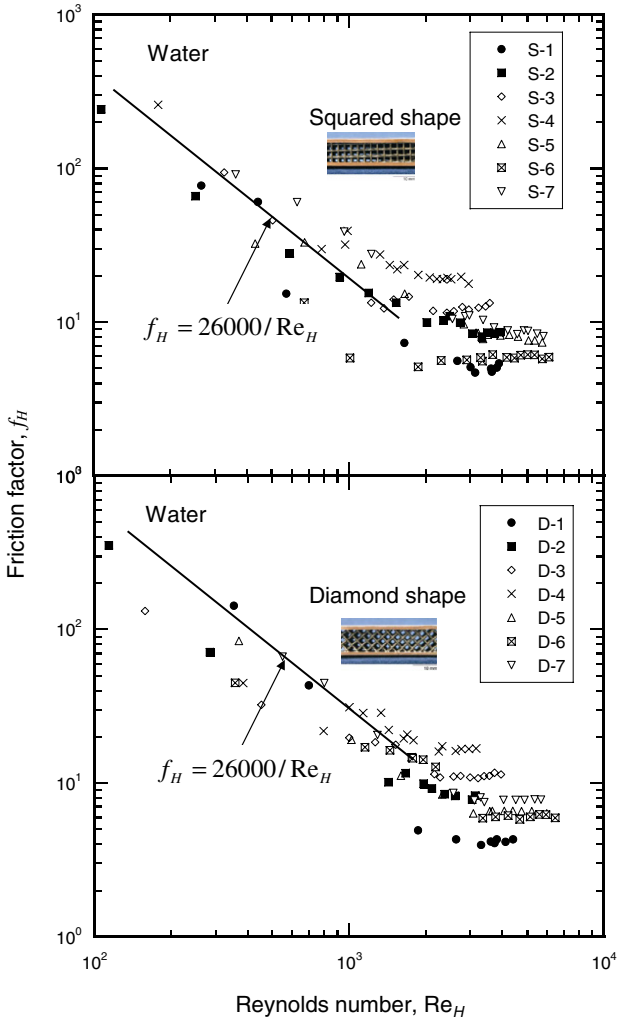

Fig. 6. Friction factors based on channel height (water as coolant).

Samples with identical wire diameter, aperture and porosity, but different core orientations (square versus diamond, samples 4 and 7) have similar friction factors using both air and water forced convections. Similar trends were observed, suggesting that square- and diamond-orientations have similar flow patterns. The difference between these two orientations is attributable mainly to the cells adjacent to the top and bottom of the sandwich panels. When the flow channel width is much larger than the channel height, the flow resistance mainly depends on flow mixing, with negligible contribution from the partial cells near the substrate walls. Hence, the core shape does not cause major difference in pressure loss.

The friction factors of samples 4 and 7 having square and diamond topologies using different coolants are compared. At high Reynolds number, it is found that only a small difference in f_H exists between the air and water coolants; which is within experimental uncertainties.

Fig. 7a shows the friction factor f_H as a function of porosity ε at a constant Reynolds number ($Re_H = 4000$). Note that the flow resistance decreases with increasing ε. Samples with a lower porosity (hence a higher relative density) have higher d/w ratios, and the frontal area of its cross-section is blocked more than that of a sample with a higher porosity. From the previous discussion on friction factor, it is noted that frontal area blockage causes large pressure losses. This is consistent with the results presented in Fig. 7a.

Because the open area ratio and porosity are both functions of d/w, the porosity can be expressed in terms of open area ratio and vice versa. The friction factors of all samples tested are plotted as functions of open area ratio, R_{open}, in Fig. 7b. The predicted pressure loss coefficient, K_{cell}, agrees very well with the experimental data. In general, friction factor increases as the open area ratio is decreased. In contrast with the data of Fig. 7a, the use of a pressure loss coefficient allows all the data fall onto a single master curve characterized by Eq. (10), whether the cell topology is square or diamond and irrespective of the porosity level. The excellent agreement between (10) and Fig. 7b demonstrates that the pressure loss coefficient is only dependent upon the open area ratio, and not on wire diameter, aperture size and cell topology. On the other hand, although the

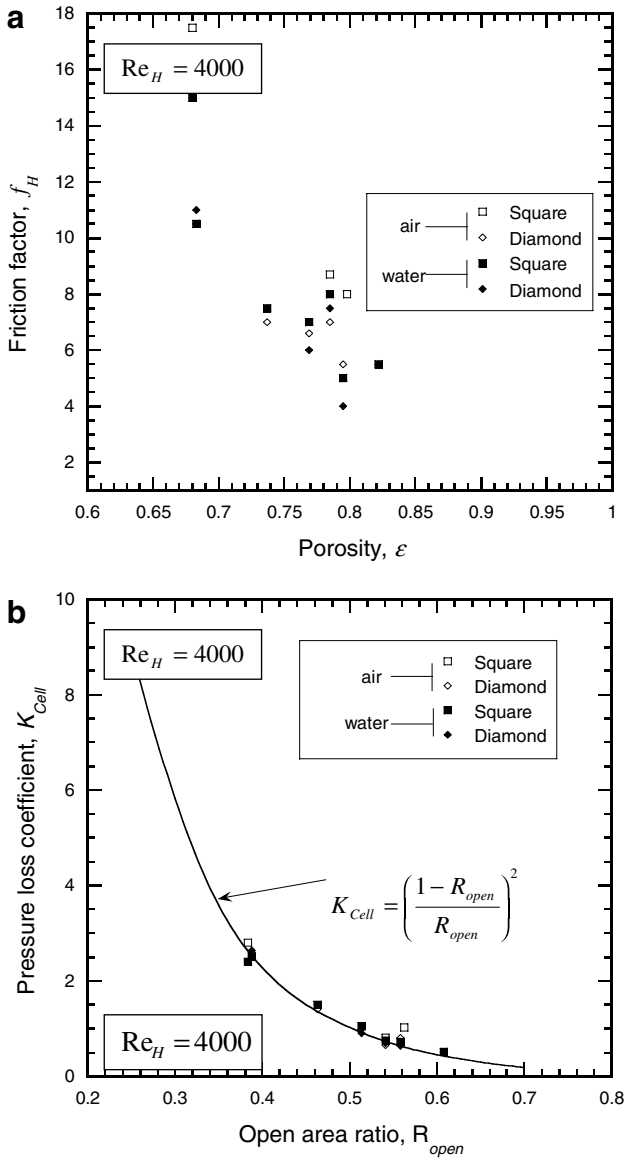

Fig. 7. (a) Effect of porosity on friction factors; (b) comparison of pressure loss coefficient predictions with measurements.

data of Fig. 7a shows that the friction factor decreases in general with increasing porosity, there is considerable scatter of data due to the additional influence of wire diameter, aperture size as well as cell topology. This explains the advantage of using K_{cell} to characterize the pressure loss across periodic lattice structures.

5.2. Heat transfer – measurements

The three main mechanisms of forced convective heat transfer through a cellular textile structure are: (1) heat transfer through solid struts by conduction; (2) heat transfer through textile core by convection; (3) heat transfer from face-sheets by convection. The overall heat transfer consists of the contribution of heat transfer from both the solid and cooling fluid. In general, increasing the thermal conductivity of the textile core increases the heat transfer by mechanism 1, increasing the surface area density enhances mechanism 2, and lowering the core relative density increases the significance of mechanism 3. An increase in the turbulence of the cooling flow causes an increase in heat transfer by mechanisms 2 and 3. Typically, increasing the porosity of a textile core increases the surface area density, and hence may increase heat transferred by mechanism 2 or 3; on the other hand, because of the high porosity, there is limited solid conduction passages (mechanism 1). It is therefore anticipated that an optimal porosity exists (balance between surface area density and relative density) that maximizes the heat transfer characteristics for textile based sandwich structures.

The heat transfer performance of all the copper and stainless steel sandwich structures is compared in Fig. 8. It is interesting to note that the porosity of wire screens tested in this study ranged from 0.68 to 0.8, significantly smaller than that of typical metal foams, which are >0.9, but much larger than that of typical packed powder beds, which are <0.35. Therefore, conduction through the solid ligaments is expected to be more important in bonded woven textile structure than that in metal foams (as well as that of packed beds without brazing), especially with high thermal conductivity materials.

Samples S-4, 7 and D-4, 7 are identical, except that the pores in the former are square-oriented while those in the latter are diamond-oriented. Because both sets of test samples had approximately the same flow resistance and flow pattern (excluding regions near the face-sheets), it is assumed that the contribution of forced convection on the overall heat transfer was the same for these samples. However, experimental data (not shown here) indicate that

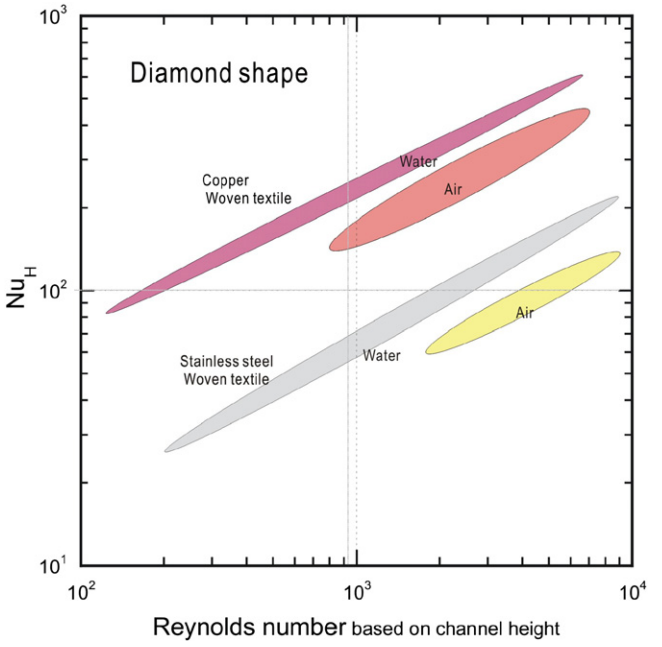

Fig. 8. Nusselt number with different solid materials and different coolants.

the Nusselt number of diamond-oriented topology is significantly higher than that of squared-oriented topology. Samples S-4 and D-4 are both made of copper, but the Nusselt number of D-4 is about 30% larger than that of S-4. This difference is mainly attributable to the different contribution from conduction through the wire ligaments. From the front view of diamond- and square-oriented samples (Fig. 2), it can be seen that the solid wire elements in the former has approximately 40% more contact area with the substrates than those in the latter, leading to a higher effective thermal conductivity in the direction of channel height. Note that this advantage is somewhat reduced because the trusses of a diamond are inclined at 45° so the thermal conduction path is longer (this effect is accounted for in the analytical model by the tortuous coefficient c_H); also, mechanism 3 will be reduced in the diamond textile by the increased (doubled) wire face-sheet contact area. However, the results of Fig. 8 suggest that the gain due to the increased core-face-sheet contact area overwhelms other lesser effects.

The experimental results presented in Fig. 8 can also be used to highlight the effect of coolant properties on the overall heat transfer of the system. Although the thermal conductivity, thermal capacity and Prandtl number of water are an order of magnitude larger than those of air, it is shown in Fig. 8 that the Nusselt number of both the copper and stainless steel textile sandwichs subjected to forced water convection is only 50–100% higher than that subjected to forced air convection. According to the heat transfer correlation for tube bundles [28], the ratio of Nusselt numbers of the two fluids depend on the ratio of Prandtl numbers of the fluids as:

$$Nu_{\text{water}}/Nu_{\text{air}} = (Pr_{\text{water}}/Pr_{\text{air}})^{0.36} \tag{21}$$

Thus, for tube bundles, heat transfer using water as the coolant is ~2.3 times larger than that of air as the coolant. For the woven textile sandwichs, (21) over-predicts the heat dissipation capability of using water as the coolant. In other words, the amount of heat dissipated by the porous structure not only depends on the Prandtl number of the coolant but also depends on other factors such as coolant conductivity, cell shape and porosity.

The effect of material conductivity on the heat transfer performance of the textile sandwich structures is illusatred in Fig. 8. Copper has a conductivity of ~380 W/K · m, which is ~20 times greater than that of stainless steel (~17 W/K · m). However, the results show that the Nusselt number for the copper sandwichs at a given Reynolds number is only about three times greater than comparable stainless steel sandwichs, whether air or water was used as the coolant flow. This is due to the fact that only a portion of the overall heat transfer rate can be attributed to solid conduction within the struts. Samples with higher porosities have less solid material, and hence the effect of solid conductivity is diminished.

Fig. 9 shows the Nusselt numbers for both copper and stainless steel diamond oriented cores as functions of relative density, for specific values of Reynolds number under forced air convection. Similar trends for the water experiments, not shown here for brevity, are also observed. The overall heat transfer rate appears to maximize around a relative density of ~0.25 for copper textile structures. However, the stainless steel samples exhibited a maximum heat transfer rate at a relative density of ~0.20. High porosity values have less solid material per unit volume, and hence less conduction through the wire ligaments. Low porosity values have less void volume per unit volume, and hence less contribution of forced convection. Therefore, an optimal porosity for maximum heat transfer exists with the precise porosity level being dependent upon parent material thermal conductivity and cell topology. In addition, it appears to be fairly independent upon the Reynolds number. For the sandwich structures tested here, this optimum porosity lies in the range between 0.7 and 0.75 for the copper textile and between 0.75 and 0.80 for

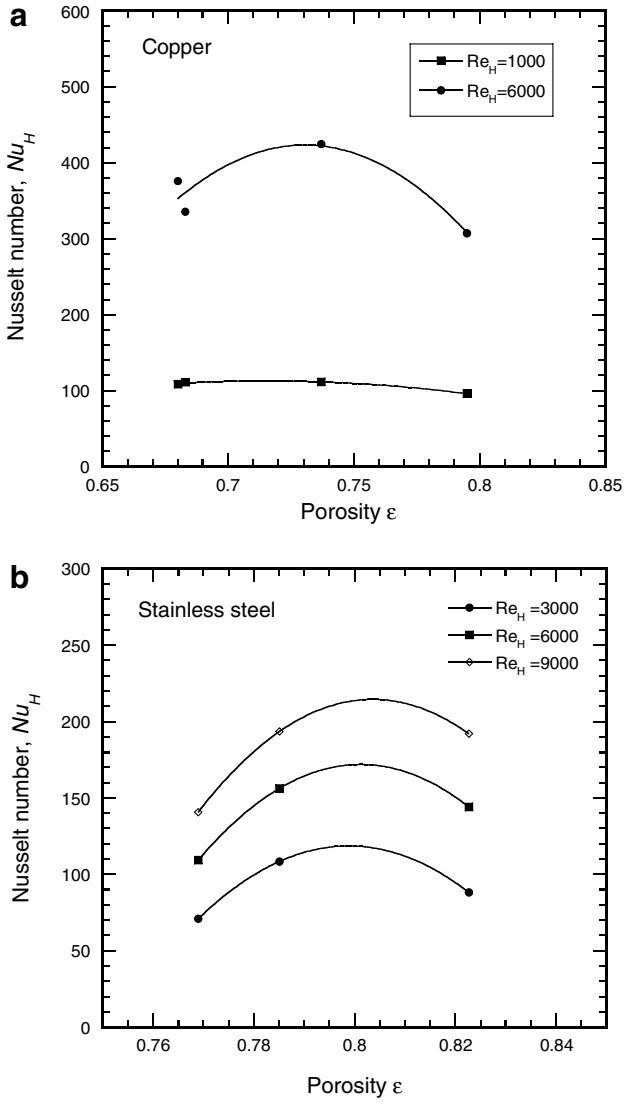

Fig. 9. Nusselt number plotted as a function of porosity for selected Reynolds numbers (air as coolant): (a) copper; (b) stainless steel.

the stainless steel textiles. Similar optimal porosity levels exist for samples with square topology. At a given porosity, the amount of heat dissipated increases with increasing surface area density because the higher surface area density corresponds to a larger surface area per unit volume between coolant fluid and textile solid, and hence more heat can be transferred by convection to the coolant fluid.

5.3. Heat transfer – predictions

The experimentally measured Nusselt numbers have been compared with predictions using the fin analogy model. In general, there is good agreement between measurement and prediction when air was used as the coolant, whereas there is significant deviation between experiment and model when water was used as the coolant (see Fig. 10a). For both square- and diamond-oriented topologies, the differences between predictions and experimental measurements were within experimental uncertainties, i.e., <10% if air is used as the coolant. For the water experiments, the current fin analogy model underestimates the heat transfer capability of textile sandwichs. The model only considers heat transferred through the fluid phase via conduction and convection. However, heat is also transferred through the fluid phase by dispersion due to the presence of fluid grains and interconnected pore system [27]. Hunt and Tien [27] experimentally found that this 'thermal dispersion' in fibrous media is significantly larger than molecular, solid conduction for high Reynolds number flows, and hence must be properly accounted for in any modelling effort. The dispersion conductivity relates to the property of coolant, porosity and flow velocity. When water was used as the coolant, it is now well known that thermal dispersion effects were pronounced [27]. In recent years, the effect of thermal dispersion has also been found to be non-negligible even in some air-flow cases. However, in the present air experiments, at least for the range of parameters considered (porosity, flow velocity), we found that this effect can be neglected without causing significant errors.

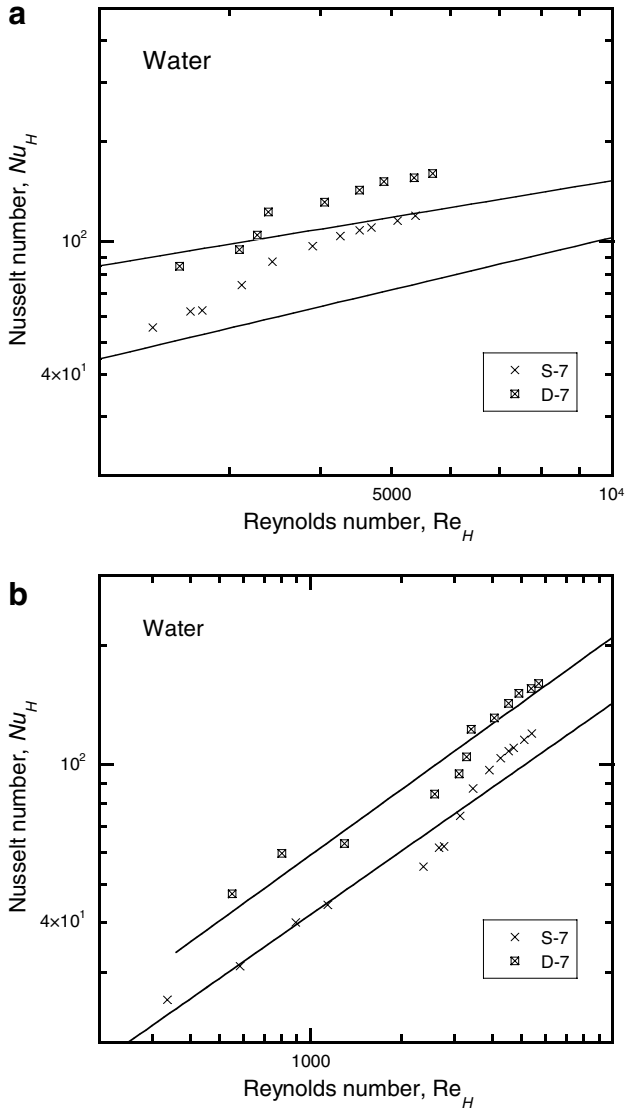

Fig. 10. Comparison of water experimental data with fin analogy model predictions: (a) without thermal dispersion effects; (b) with thermal dispersion effects.

Consequently, for water experiments, additional effects due to thermal dispersion must be included in the fin analogy model. Thermal dispersion in porous media is caused by the effect of pore-level velocity non-uniformity on the pore-level temperature distribution, leading to enhanced heat transfer (i.e., the dispersion contribution is larger than the molecular diffusion) when the Peclet number $Pe = Re\,Pr$ is sufficiently large [27,35,36]. The pore structure (ordered versus disordered), pore velocity and upstream flow conditions determine whether the pore-level hydrodynamics are recirculation zones (closed streamlines), dead ends, flow reversals, etc. Although several flow regimes exist in the pore depending on the pore Reynolds number Re, it has been found experimentally that the Re dependence is rather weak, with the pore-level hydrodynamics approximately characterized by Pe [36]. Therefore, the thermal dispersion conductivity, k_d, is often defined as [27,41]:

$$k_d = CRe_d Prk_f \tag{22}$$

where C is a non-dimensional coefficient, and $Re_d = \rho_f U_m d/\mu_f$, with d representing the wire diameter.

It is expected that the transfer of heat through textile sandwichs would be enhanced by thermal dispersion caused by fluid temperature differences perpendicular to the direction of coolant flow. Hence, in Eq. (12), the solid and fluid temperatures should be functions of the local coordinate ξ, leading to:

$$\frac{d^2T}{d\xi^2} - \frac{4h}{k_s d}(T(\xi,x) - T_f(\xi,x)) = 0 \tag{23}$$

Because both solid and fluid temperatures are unknown quantities, (23) is difficult to solve.

To simplify the problem, it is assumed that heat transferred by thermal dispersion is achieved by a fluid with enhanced thermal conductivity k_d. This mechanism is similar to heat transferred through the solid struts by conduction. Therefore, the amount of heat transferred between the solid struts and coolant fluid may be divided into two parts, i.e., heat transferred between the solid strut and fluid (of conductivity k_d) by conduction and that by convection. These two processes can be described by:

$$\frac{d^2T}{d\xi^2} - \frac{4h}{k_s d}(T(\xi, x) - T_d(\xi, x)) = 0 \tag{24a}$$

$$\frac{d^2T}{d\xi^2} - \frac{2h}{k_d d}(T_d(\xi, x) - T_f(x)) = 0 \tag{24b}$$

where T_d is the fluid temperature around wire struts due to thermal dispersion, called dispersion temperature, and T_f is the fluid temperature away from the cell ligaments. The different factors appearing in (24a and 24b) are due to the fact that the surface of heat transfer in the case of (24a) is the circular cross-section of the cylinder whereas that in (24b) is the cylindrical surface of the cylinder. The corresponding boundary conditions are:

$$\begin{aligned} -k_s\frac{dT}{d\xi}\Big|_{\xi=0} &= q, \quad k_s\frac{dT}{d\xi}\Big|_{\xi=C_H H} = 0, \\ -k_d\frac{dT_d}{d\xi}\Big|_{\xi=0} &= q, \quad k_d\frac{dT_d}{d\xi}\Big|_{\xi=C_H H} = 0 \end{aligned} \tag{25}$$

Finally, with the above model, the (non-dimensional) temperature difference between solid and fluid is obtained as:

$$\begin{aligned} \Theta = {} & \frac{e^{m\xi}}{1-e^{2mC_H H}}\left[\frac{mq}{(m^2-m_1^2)k_d} - \frac{q}{mk_s}\right] \\ & + \frac{e^{2mC_H H}}{1-e^{2mC_H H}}\left[\frac{mq}{(m^2-m_1^2)k_d} - \frac{q}{mk_s}\right]e^{-m\xi} \\ & + \frac{m^2 q e^{m_1\xi}}{(m^2-m_1^2)m_1 k_d(e^{2m_1 C_H H}-1)} \\ & + \frac{m^2 q e^{2m_1 C_H H - m_1\xi}}{(m^2-m_1^2)m_1 k_d(e^{2m_1 C_H H}-1)} \end{aligned} \tag{26}$$

whereas the wall temperature at the bottom face-sheet is:

$$\begin{aligned} T_w - T_f = {} & \left[\frac{q}{mk_s} - \frac{mq}{(m^2-m_1^2)k_d}\right]\frac{\cosh(mC_H H)}{\sinh(mC_H H)} \\ & + \frac{m^2 q}{(m^2-m_1^2)m_1 k_d}\frac{\cosh(m_1 C_H H)}{\sinh(m_1 C_H H)} \end{aligned} \tag{27}$$

Eqs. (26) and (27) can now be substituted for (14) and (15) in the fin analogy model.

After incorporating thermal dispersion effects in the fin analogy model, the predicted Nusselt number values for forced water convection experiments are in good agreement with experimental results, as shown in Fig. 10b.

5.4. Discussion

In this section, the parameters that affect the heat transfer performance of textile based sandwich structures are studied. Because the trends of square- and diamond-oriented topologies were similar (as far as the effects of wire diameter, aperture size and porosity on heat transfer are concerned), for the sake of brevity, only the square-oriented topology was considered; the results are readily applicable to diamond topologies which have superior mechanical properties than the square ones [4,6]. For simplicity, all the discussions are based on results obtained for forced air convection.

5.4.1. Effect of solid conductivity

The effect of thermal conductivity of the parent solid material on the overall thermal performance of brazed textile based sandwich structures (at a Reynolds number of

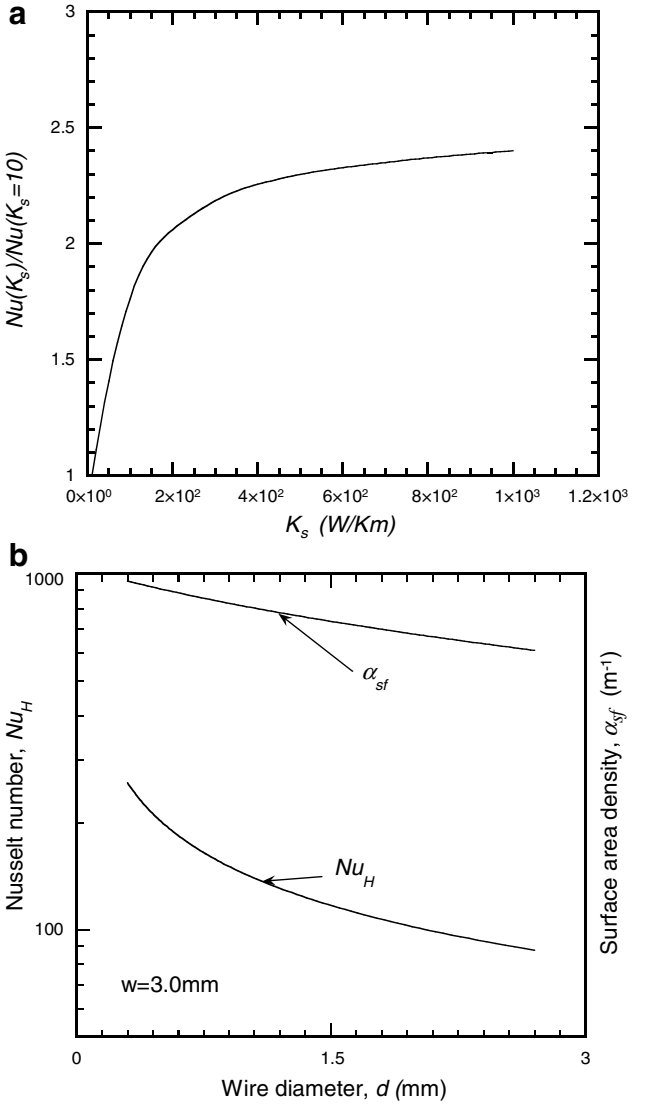

Fig. 11. Effect of (a) solid thermal conductivity and (b) wire diameter on heat transfer (air as coolant).

5000) is shown in Fig. 11a. Here, the ordinate axis is the Nusselt number at arbitrary solid conductivity k_s normalized by the Nusselt number at $k_s = 10$ W/mK It can be seen from Fig. 11a that the heat transfer rate increases sharply with increasing k_s when it is less than $\sim$100 W/K · m. Subsequently, the rate of increase slows down, gradually reaching a plateau when k_s is larger than a critical value of $\sim$300 W/mK. That is to say, when the solid conductivity reaches its critical value, a further increase does not lead to significant increases in the overall heat transfer rate. In general, this critical conductivity value is not a constant but depends somewhat on parameters such as the Reynolds number, coolant type, cellular topology, cell size and core height. For example, it is expected that the critical conductivity decreases with decreasing cell size and increases as the core height is increased. However, these deviations are in general small, with the critical conductivity lying approximately in the range of 300–400 W/mK.

5.4.2. Effect of wire diameter

To highlight the effect of varying wire diameter d on the heat transfer performance, the aperture size in this section is fixed at $w = 3$ mm and the Reynolds number at $Re_H = 5000$. Under these conditions, Fig. 11b shows the surface area density and Nusselt number as functions of the wire diameter. It can be seen that increasing the wire diameter leads to a decrease in α_{sf} and Nu_H, which in turn decreases the overall heat transfer rate. Note that the overall heat transfer performance depends on both conduction and convection mechanisms. With a fixed aperture size, increasing the wire diameter increases the volume fraction of solid material and hence the contribution of conduction to the overall heat transfer would increase. However, the surface area density drops dramatically with increasing wire diameter, leading to a reduced contribution from convection. For the conditions examined here the decrease in convection is greater than the increase in conduction, and hence the overall heat transfer rate decreases.

5.4.3. Effect of aperture size

Our results (not included here) show that, for fixed values of Reynolds number and wire diameter, the Nusselt number is inversely proportional to aperture size. That is, as the aperture size is increased, the porosity increases and the surface area density decreases, which results in a decrease in the conduction and convection mechanisms. As a result, the overall heat transfer rate decreases.

5.4.4. Effect of surface area density

From previous discussions, it is noted that porosity (or relative density) and surface area density are two important geometrical parameters governing overall heat transfer. Therefore, in this and the next section, the focus will be placed on these two characteristics.

At a fixed porosity of $\varepsilon = 0.8$ and a fixed Reynolds number of $Re_H = 5000$, Fig. 12a shows the variation of Nusselt number with surface area density. It is seen from this figure

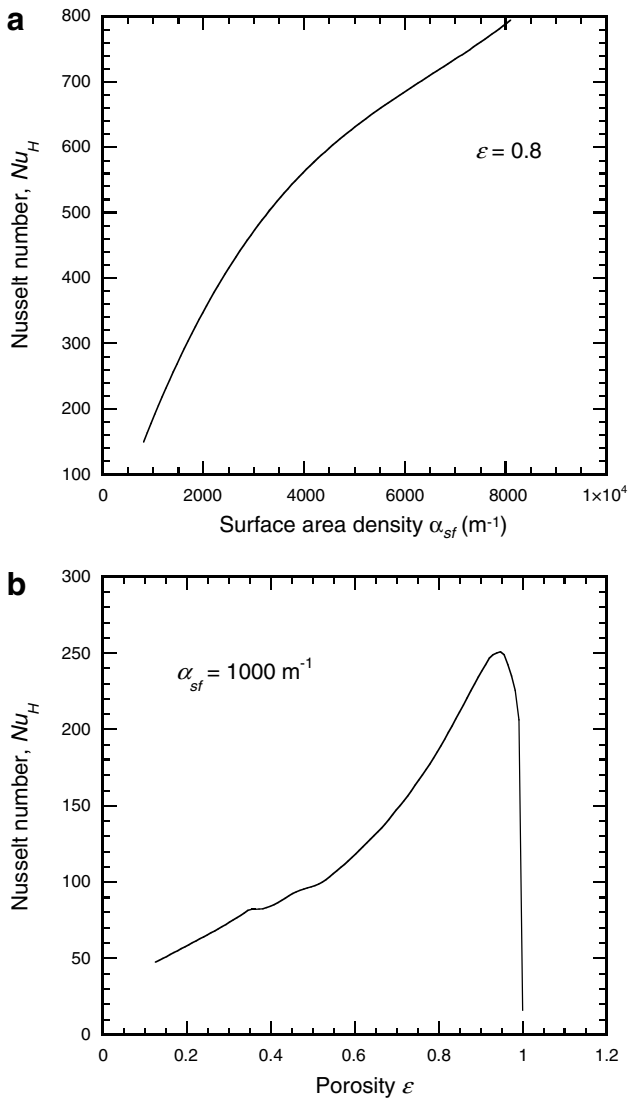

Fig. 12. Effect of (a) surface area density and (b) porosity on heat transfer (air as coolant).

that the Nusselt number increases with increasing surface area density. With a fixed porosity, the amount of solid material per unit volume is fixed, and hence the overall heat transfer rate only varies with the convection mechanisms. A higher surface area density increases the convection contribution due to a larger available surface area per unit volume.

5.4.5. Effect of porosity

The effect of the porosity on heat transfer in plotted in Fig. 12b, for $\alpha_{sf} = 1000\ \mathrm{m}^{-1}$ and $Re_H = 5000$. In the extreme case when the porosity is 1.0, heat transfer consists solely of convection from the face sheets; whereas in the case of zero porosity, heat transfer consists solely of conduction through a solid block of material. Increasing the porosity leads to less conduction due to the reduction of solid material per unit volume, whereas the contribution of convection increases. The overall thermal performance

depends on the balance of both thermal conduction and convection mechanism. As a result, there exists an optimal porosity for maximum heat transfer as shown in Fig. 12b. When the porosity exceeds 0.9, the small amount of solid material in the textile core cannot create secondary flows (which improve convective heat transfer) and the overall Nusselt number drops dramatically.

6. Comparison with other heat exchanger media

The brazed copper and stainless steel textile based sandwichs are compared with the following types of heat exchanger medium: investment cast lattice-frame materials (LFMs, aluminium alloy) [29–35], investment cast Kagome structures (bronze) [42], metal foams (copper and FeCrAlY – a steel alloy) fabricated via solid state sintering [36,37], investment cast aluminium foams [39], folded aluminium louver fin arrays [30], and corrugated ducts with sinusoidal wavy passages [40]; in addition an empty channel was also included. All were evaluated under forced air convection.

6.1. Pressure loss

The comparison of the overall pressure loss or friction factor through different heat dissipation media is shown in Fig. 13 for a wide range of Reynolds numbers. Flow through powder packed beds experiences the highest drag, because they have the lowest porosity compared with other porous media considered [37]. The typical flow resistance of metal foams are about two orders of magnitude greater than that of an empty channel [32]. In most cases, the friction factor of metal foams are also greater than that of periodic materials such as textiles [7], Kagome structures [42] and LFMs [30], even though the porosity of foams is higher (comparable with Kagome and LFM structures, but significantly higher than the textile). This indicates that the main difference between stochastic and periodic materials is due to the difference in flow patterns. For stochastic materials, the main characteristics are porosity and pore size [34].

The flow resistance of LFMs and Kagome structures is about 10 times higher than that of an empty channel, but lower than that of textile lattice structures. Although both topologies are periodic they have different porosities, with

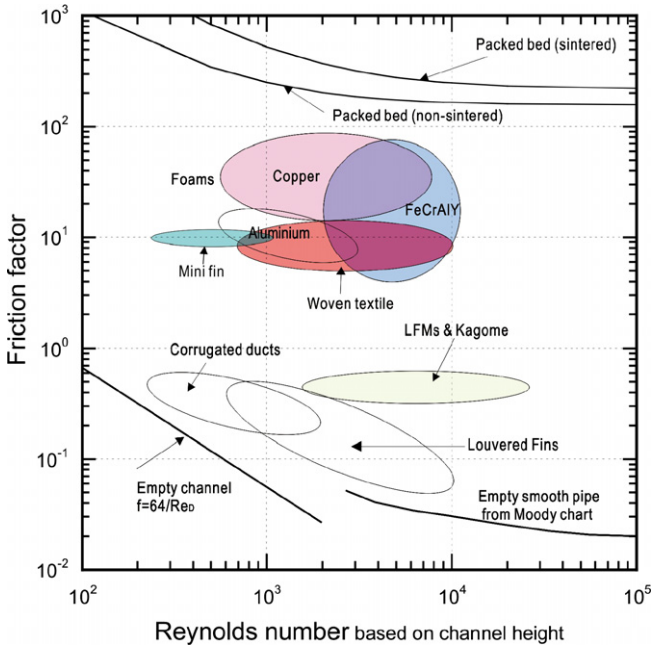

Fig. 13. Friction factor of brazed textile structures compared with other heat dissipation media.

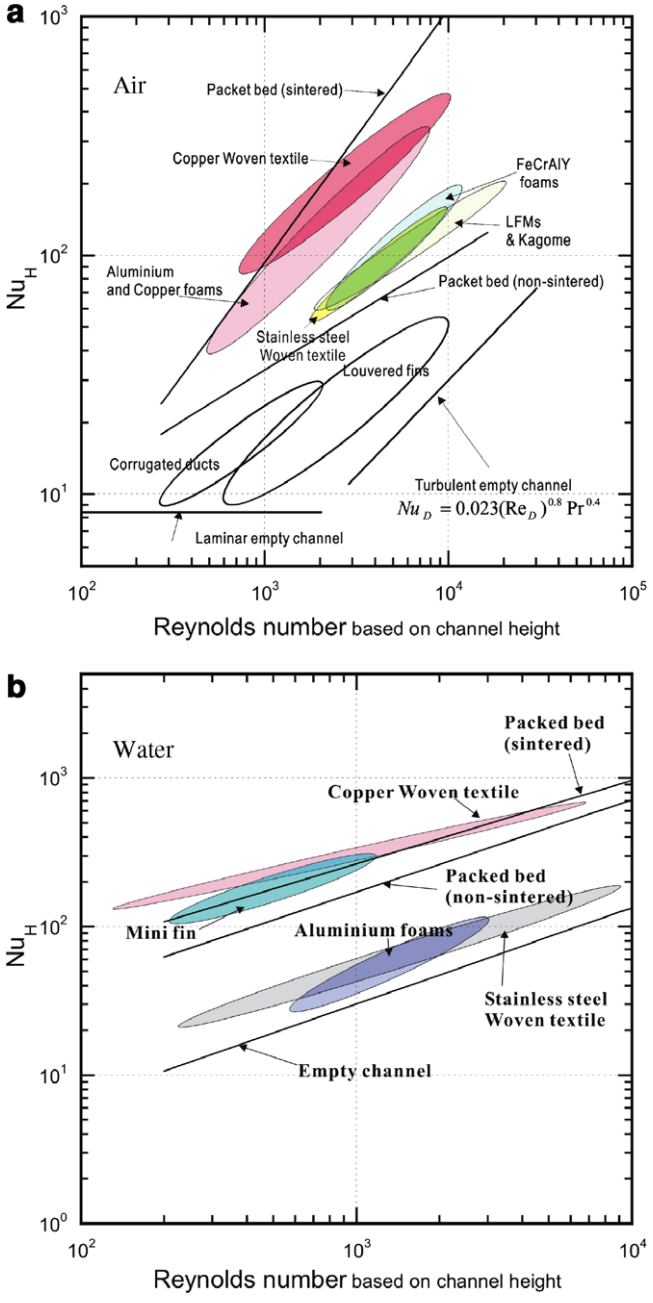

Fig. 14. Heat transfer performance of brazed textile structures compared with other heat dissipation media: (a) air as coolant; (b) water as coolant.

$\varepsilon = 0.7$–0.8 for the textiles and $\varepsilon \sim 0.9$ for the LFMs and Kagome structures. The friction factor of mini fins (which has a porosity of 0.8) is comparable to that of the textile structures [43]. For periodic materials, porosity (as well as pore size) is the main characteristic dictating pressure loss; other factors such as tortuosity and cell shape are expected to be secondary.

6.2. Heat transfer

Fig. 14a and b compare the overall heat transfer performance of different heat dissipation media for forced air and water convection, respectively. From the data, it is seen that copper and stainless steel textile structures, aluminium and copper foams, copper mini fins and sintered bronze packed beds outperform corrugated duct and louvered fin structures. This is attributed to the contribution of conduction through the network of solid ligaments in addition to forced convection, whereas corrugated duct and louvered fin structures depend mainly on the change in flow patterns caused by augmented heat transfer surfaces (convection). For air experiments, the copper textiles had porosities close to the optimal level ($\varepsilon \approx 0.75$). Because of the high porosity ($\varepsilon > 0.9$) of aluminium and copper foams, the contribution of solid conduction to the overall heat transfer was not as pronounced in comparison of that due to forced convection. The stainless steel textiles have a similar heat transfer rate as FeCrAlY foams, LFMs and Kagome structures. For the packed beds, the high thermal contact resistance of the non-sintered structure causes a significant knockdown in the heat transfer performance compared to that of sintered structures.

In the water experiments, the copper textiles have similar heat transfer rates when compared to the copper mini fin structures and bronze sintered packed beds, whereas the heat transfer rates of the stainless steel textiles are comparable to the open-cell aluminium foams.

7. Conclusions

The overall pressure drop and heat transfer performance of brazed copper and stainless steel periodic textile-based lattice structures were experimentally investigated under steady-state forced convection conditions, using both air and water as the coolant. Prototype sandwich structures with different topologies were fabricated and tested.

At high Reynolds numbers, fluid flow in the textile structures is form dominated. The friction factor based on unit pore size depends mainly on the open area ratio. The transfer of heat depends on two competing mechanisms: conduction through the solid ligaments and forced convection to the applied coolant flow. The heat transfer performances of diamond oriented structures is superior to square-oriented structures for samples of similar porosity and surface area density. At a given Reynolds number, porosity and surface area density are the two key parameters controlling heat transfer. At a given porosity, the heat dissipation rate increases as the surface area density is increased. However, for a fixed surface area density, an optimal porosity exists for maximum heat dissipation (a balance between the two mechanisms). For copper textile structures, this optimal porosity is about 0.75. A fin analogy model has been developed and successfully used to predict the heat transfer performance under forced air convection. For the water experiments, however, the model must be modified to account for the effects of thermal dispersion.

Performance charts are presented to compare textile structures with selected heat dissipation media. Thermally, the copper textile structures perform as well as the stochastic open-celled metal foams (aluminium and copper based), both having large surface area densities. However, the pumping power required is significantly lower for the textile-based structures, because of the periodic topology. Therefore, their overall thermal efficiency is about 3 times greater than that of comparable weight open-celled copper foams.

Acknowledgements

This work was supported by the National Basic Research Program of China (2006CB601202), the National 111 project (B06024), by the National Natural Science Foundation of China (10328203, 10572111, 10632060), and by the US Office of Naval Research (N000140110271). The authors would like to thank Prof. P.X. Jiang of Tsinghua University, China, for help in the forced water convection experiments.

References

[1] A.G. Evans, J.W. Hutchinson, M.F. Ashby, Multifunctionality of cellular metal systems, Prog. Mater. Sci. 43 (1999) 71–221.
[2] J.S. Liu, T.J. Lu, Multi-objective and multi-loading optimization of ultralightweight truss materials, Int. J. Solids Struct. 41 (2004) 619–635.
[3] N. Wicks, J.W. Hutchinson, Optimal truss plates, Int. J. Solids Struct. 38 (2001) 5165–5183.
[4] D.J. Sypeck, H.N.G. Wadley, Multifunctional microtruss laminates: textile synthesis and properties, J. Mater. Res. 16 (2001) 890–897.
[5] H.N.G. Wadley, Cellular metals manufacturing, Adv. Eng. Mater. 4 (2002) 726–733.
[6] A.G. Evans, J.W. Hutchinson, N.A. Fleck, M.F. Ashby, H.N.G. Wadley, The topological design of multifunctional cellular metals, Prog. Mater. Sci. 46 (2001) 309–327.
[7] J. Tian, T. Kim, T.J. Lu, H.P. Hodson, D.T. Queheillalt, D.J. Sypeck, H.N.G. Wadley, The effects of topology upon fluid-flow and heat-transfer within cellular copper structures, Int. J. Heat Mass Transfer 47 (2004) 3171–3186.
[8] W.M. Kays, A.L. London, Compact Heat Exchangers, 3rd ed., McGraw-Hill, 1984.
[9] J.W. Park, D. Ruch, R.A. Wirtz, Thermal/fluid characteristics of isotropic plain-weave screens laminates as heat exchanger surfaces, AIAA paper 2002–0208, AIAA Aerospace Sciences Meeting, Reno, NV, Han, 2002.
[10] R.A. Wirtz, J. Xu, J.W. Park, D. Ruch, Thermal/Fluid Characteristics of 3d Woven Mesh Structures as Heat Exchanger Surfaces, paper no. 1372, Itherm, San Diego, 2002, pp. 307–314.

[11] R.A. Wirtz, C. Li, J.W. Park, J. Xu, High performance woven mesh heat exchangers, Eleventh AIAA/MDA Technology Conference and Exhibit Monterey CA, 2002.
[12] J. Xu, R.A. Wirtz, In-plane effective thermal conductivity of plain-weave screen laminates, Thermal Challenges in Next Generation Electronic Systems, Millpress, Rotterdam, IEEE CPTT Journal, 2002.
[13] C. Li, R.A. Wirtz, Development of a high performance heat sink based on screen-fin technology, Ninteenth IEEE Semi-Therm, IEE 03 CH37437, 2003, pp. 53–60.
[14] J.R. Sodré, J.A.R. Parise, Friction factor determination for flow through finite wire-mesh woven-screen matrices, ASME J. Fluid Eng. 119 (1997) 847–851.
[15] D. Mehta, M.A. Hawley, Wall effect in packed columns, I &EC Process Design and Development 8 (1969) 280–282.
[16] S. Ergun, Fluid flow trough packed columns, Chem. Eng. Prog. 48 (1952) 89–94.
[17] A. Ahmad, J. Saini, H. Varma, Effect of geometrical and thermo-physical characteristics of bed materials on the enhancement of thermal performance of packed-bed solar air heaters, Energ. Convers. Manage. 36 (1995) 1185–1195.
[18] F. Duprat, G. Lopez, Comparison of performance of heat regenerators: relation between heat transfer efficiency and pressure drop, Int. J. Energ. Res. 25 (2001) 319–329.
[19] W.S. Chang, Porosity and effective thermal conductivity of wire screens, ASME J. Heat Tran. 112 (1990) 5–9.
[20] C.T. Hsu, K.W. Wong, P. Cheng, Effective stagnant thermal conductivity of wire screen, J. Thermophys. 10 (1996) 542–545.
[21] P.X. Jiang, M. Li, T.J. Lu, Y. Yu, Z. P Zen, Experimental research on convection heat transfer in sintered porous plate channels, Int. J. Heat Mass Transfer 47 (2004) 2085–2096.
[22] T.J. Lu, H.A. Stone, M.F. Ashby, Heat transfer in open-cell metal foams, Acta mater 46 (1998) 3619–3635.
[23] T.J. Lu, Heat transfer efficiency of metal honeycombs, Int. J. Heat Mass Transfer 42 (1999) 2031–2040.
[24] S. Gu, T.J. Lu, A.G. Evans, On the design of two-dimensional cellular metals for combined heat dissipation and structural load capacity, Int. J. Heat Mass Transfer 44 (2001) 2163–2175.
[25] C.Y. Zhao, T.J. Lu, Analysis of microchannel heat sinks for electronics cooling, Int. J. Heat Mass Transfer 45 (2002) 4857–4869.
[26] T. Kim, C.Y. Zhao, T.J. Lu, H.P. Hodson, Convective heat dissipation with lattice-frame materials, Mech. Mater. 36 (2004) 767–780.
[27] M. Hunt, C. Tien, Effects of thermal dispersion on forced convection in fibrous media, Int. J. Heat Mass Transfer 31 (1988) 301–309.
[28] A.A. Zukauskas, Convective heat transfer in, cross-flow, in: Handbook of Single-Phase Heat Transfer, Wiley, New York, 1987.
[29] T. Kim, A.J. Fuller, H.P. Hodson, T.J. Lu, An experimental study on thermal transport in lightweight metal foams at high Reynolds numbers, in: Proceedings of the International Symposium of Compact Heat Exchangers, Grenobel, France, 2002, pp. 227–232.
[30] T. Kim, Fluid-Flow and Heat-Transfer in a Lattice-Frame Material, PhD Thesis, Department of Engineering, University of Cambridge, 2003.
[31] T. Kim, H.P. Hodson, T.J. Lu, Fluid-flow and endwall heat-transfer characteristics of an ultralight lattice-frame material, Int. J. Heat Mass Transfer 47 (2004) 1129–1140.
[32] C.Y. Zhao, Thermal Transport in Cellular Metal Foams with Open Cells, PhD Thesis, Department of Engineering, University of Cambridge, 2003.
[33] C.Y. Zhao, T. Kim, T.J. Lu, H.P. Hodson, Thermal transport in high porosity cellular metal foams, J. Thermofluid Phys. 18 (2004) 901–911.
[34] A. Amiri, K. Vafai, Analysis of dispersion effects and non-thermal equilibrium non-Darcian variable porosity incompressible flow through porous media, Int. J. Heat Mass Transfer 37 (1994) 939–954.
[35] C. Hsu, P. Cheng, Thermal dispersion in a porous medium, Int. J. Heat Mass Transfer 33 (1990) 1587–1597.
[36] M. Kaviany, Principles of Heat Transfer in Porous Media, Springer, New York, 1995.
[37] M. Li, Numerical and Experimental Research of Heat Transfer in Porous Media, Master degree thesis, Tsinghua University, PR China, 2002.
[38] H.W. Coleman, W.G. Steels, Experimentation and Uncertainty Analysis for Engineers, 2nd ed., John Wiley & Sons Inc., 1999.
[39] S.Y. Kim, B.H. Kang, J.H. Kim, Forced convection from aluminium foams in an asymmetrically heated channel, Int. J. Heat Mass Transfer 44 (2001) 1451–1454.
[40] H. Blomerius, C. Holsken, N.K. Mitra, Numerical investigation of flow field and heat transfer in cross-corrugated ducts, ASME J. Heat Tran. 121 (1999) 314–321.
[41] F.W. Dittus, L.M.K. Boelter, Heat transfer in automobile radiators of the tubular type, University of California Publications in Engineering 2 (1930) 443–461.
[42] F. Hoffmann, T.J. Lu, H.P. Hodson, Heat transfer performance of Kagome structures, In: Proceedings of the eighth UK National Heat Transfer Conference, Oxford, 9–10 September, 2003.
[43] P.X. Jiang et al., Experimental investigation of convection heat transfer in mini-fin structures and sintered porous media, J. Enhanced Heat Tran. 11 (2004) 391–405.
[44] P.X. Jiang, M. Li, Y.C. Ma, Z.P. Ren, Boundary conditions and wall effect for forced convection heat transfer in sintered porous plate channels, Int. J Heat Mass Transfer 47 (2004) 2073–2083.